Energy of Dissociation of Lipid Bilayer from the Membrane Skeleton of Red Blood Cells

William C. Hwang* and Richard E. Waugh#
*Department of Biochemistry and Biophysics, and #Department of Pharmacology and Physiology, University of Rochester School of Medicine and Dentistry, Rochester, New York 14642 USA

ABSTRACT The association between the lipid bilayer and the membrane skeleton is important to cell function. In red blood cells, defects in this association can lead to various forms of hemolytic anemia. Although proteins involved in this association have been well characterized biochemically, the physical strength of this association is only beginning to be studied. Formation of a small cylindrical strand of membrane material (tether) from the membrane involves separation of the lipid bilayer from the membrane skeleton. By measuring the force required to form a tether, and knowing the contribution to the force due to the deformation of a lipid bilayer, it is possible to calculate the additional contribution to the work of tether formation due to the separation of membrane skeleton from the lipid bilayer. In the present study, we measured the tethering force during tether formation using a microcantilever (a thin, flexible glass fiber) as a force transducer. Numerical calculations of the red cell contour were performed to examine how the shape of the contour affects the calculation of tether radius, and subsequently separation work per unit area W_{sk} and bending stiffness k_c. At high aspiration pressure and small external force, the red cell contour can be accurately modeled as a sphere, but at low aspiration pressure and large external force, the contour deviates from a sphere and may affect the calculation. Based on an energy balance and numerical calculations of the cell contour, values of the membrane bending stiffness $k_c = 2.0 \times 10^{-19}$ Nm and the separation work per unit area $W_{sk} = 0.06$ mJ/m^2 were obtained.

INTRODUCTION

The fluid character of the membrane bilayer is well known. Although it is clear that this fluid character necessitates associations with an elastic cytoskeleton to ensure control over bilayer membrane shape and stability, the precise nature of the associations between bilayer and skeleton remains obscure for most cells. Even in cells for which molecular associations between integral proteins and underlying elastic elements are well known (e.g., red blood cells), the precise mechanism by which these interactions stabilize the surface against fragmentation and loss of bilayer are not well understood. Although it is true to some extent for all cells, it is particularly true for red blood cells that the strength of the association between the bilayer and the underlying membrane-associated cytoskeleton is fundamentally important for cell function. The fixed area of the red cell bilayer places strict limits on red cell deformability. Loss of bilayer area reduces cellular deformability and, if enough area is lost, leads to the destruction of the cell and its removal from circulation (Waugh et al., 1992a).

The red cell membrane is a good system for studying bilayer skeletal associations, not only because of its physiological relevance, but also because of the wealth of structural and biochemical information we have about the red cell. The membrane bilayer and underlying membrane skeleton are coupled by specific molecular interactions. One of the major interactions takes place through associations between the integral membrane protein band 3 and the membrane skeletal protein spectrin mediated by ankyrin (Bennett and Stenbuck, 1979). A second set of interactions exists between another integral membrane protein glycophorin C and the junctional complex of the membrane skeleton formed by various skeletal proteins: spectrin, actin, protein 4.1, and adducin (Pinder et al., 1993). Defects or deficiencies of proteins involved in these associations can lead to various forms of hemolytic anemia (Palek and Lambert, 1990). For example, defects in ankyrin and associated deficiencies in the concentration of spectrin on the membrane have been shown to result in hereditary spherocytosis (HS) (Palek and Lambert, 1990; Waugh and Agre, 1988).

A micromechanical approach to the study of the physical characteristics of the bilayer-skeletal association involves the formation of a small strand of membrane material (tether) from red blood cell membrane. Various evidence suggests that formation of a tether involves the separation of the lipid bilayer from the membrane skeleton (Waugh and Bauserman, 1995). First, tethers can be formed from pure lipid bilayers. No membrane skeleton is required during this process. Second, when tethers formed from red cells were fixed with glutaraldehyde and labeled with both fluorescent lipid labels (DiI) and fluorescent membrane protein labels (eosin maleimide, a band 3 label), only the lipid labels were detectable on the tether. Third, tethers are soluble in the detergent Triton X-100, whereas the membrane skeleton is not. Thus, by measuring the force required to form a tether,

Received for publication 2 December 1996 and in final form 8 March 1997.
Address reprint requests to Dr. William C. Hwang, c/o Dr. Richard E. Waugh, Department of Pharmacology and Physiology, University of Rochester School of Medicine and Dentistry, 601 Elmwood Avenue, Box 711, Rochester, NY 14642-0001. Tel.: 716-275-3768; Fax: 716-275-6007; E-mail: waugh@seas.rochester.edu.

0006-3495/97/06/2669/10 $2.00

it is possible to calculate the energy required to dissociate the lipid bilayer from the membrane skeleton.

In the present study, a microcantilever (a thin flexible glass fiber) was used as a force transducer to measure the tethering force as a function of the tether length and the velocity of tether formation. This method provides a direct measurement of the mechanical work of tether formation. In general, this work includes both conservative (elastic, reversible) and dissipative (frictional) contributions. A reversible component of the work was observed. This work is attributable in part to the energy required to bend the membrane bilayer and, in red cells, the additional work of separation due to the presence of the membrane skeleton and integral proteins. An analysis of the equilibrium state enabled us to calculate the bending modulus of the membrane bilayer and to estimate the additional contribution attributable to the presence of the membrane skeleton and integral membrane proteins.

MATERIALS AND METHODS

General procedure

To form tethers from red cells, the cells were suspended with latex beads coated with antibodies raised in rabbits against human red blood cells. The beads and cells were placed in a small cuvette on the stage of an inverted microscope. The beads adhered to the cells, and a cell-bead pair was selected for measurement. The cell was aspirated into a micropipette, and the cell-bead pair was manipulated so that the bead became caught in a V-shaped crotch at the tip of a calibrated glass microcantilever. The cell was withdrawn at a controlled rate until a tether formed between the cell body and the adherent bead. The microcantilever was deflected and the force on the tether could be determined from the deflection (Fig. 1). The procedure was recorded on videotape for subsequent analysis. The cell diameter, the length of the projection in the pipette, the tether length, the fiber deflection, and the aspiration pressure used to hold the cell in the pipette were recorded as functions of time. Two types of protocols were used. In dynamic tests, tethers were formed at different constant velocities, and the force (based on the cantilever deflection) was observed as a function of tether length and time. Alternatively, tethers of different lengths were formed, and the relaxation of the force was measured as a function of time at fixed tether length.

Preparation of red blood cells

Red blood cells were collected from healthy donors by venipuncture into heparin tubes or by finger prick. Red blood cells were then suspended at low concentration in hypotonic phosphate-buffered saline (PBS) (86.8 mM NaCl, 13.6 mM Na_2HPO_4, 3.4 mM KH_2PO_4, pH 7.3, 160 mOsm/kg) containing 5% autologous plasma.

Preparation of latex bead

Latex amino-beads (Polysciences, Warrington, PA) (0.2 ml) were washed three times with 0.25 M PO_4 (NaH_2PO_4 and Na_2HPO_4 mixed in portion to produce pH 7.5) at pH 7.5. Then an equal volume of glutaraldehyde was added and mixed overnight at 37°C, pH 7.2–7.6. On the second day, the beads were washed extensively (six times or more) with 0.25 M PO_4 and then placed in buffer containing rabbit–anti-human red cell IgG (2 mg/ml, diluted from 20 mg/ml with 0.5 M PO_4) (Cappel, Organon Teknika Corporation, Durham, NC). Beads and antibodies were mixed overnight at room temperature. Beads were then washed two times in 0.25 M PO_4, one time in 1 M NaCl, and one time in 0.05 M PO_4, then suspended in a 10× volume of 100 mM ethanolamine (pH 7.5) and kept at room temperature for 4 h to inactivate unreacted aldehyde groups. The beads were then washed two times in PBS and stored in PBS at 4°C. Beads kept in storage remained active for up to 3 months.

Preparation of chambers

Chambers consisted of a plastic spacer (~1 mm in thickness) held between two coverslips with silicon grease (Dow Corning, Midland, MI). The chamber had two openings perpendicular to each other for simultaneous access of the pipette and the microcantilever.

Preparation of micropipettes

Micropipettes were pulled from glass capillaries (Friedrich and Dimmock, Millville, NJ) using a pipette puller (Kopf, Tujunga, CA). Pipette tips were then fractured to the desired size and geometry by a microforge. Before the experiment, the interior of the pipette was filled with PBS of the same concentration as that used in cell suspension. Two different sizes of pipettes were used during the experiment. A large pipette (4-μm inside diameter) was used for microcantilever calibration. A smaller pipette (2–3-μm inside diameter) was used during tether formation.

Fabrication of microcantilevers

A small glass fiber (1 μm in diameter or less) was pulled from glass capillaries using the pipette puller. A second small piece of curved fiber was first cemented to the tip of the first fiber with methacrylate cement. Then the two pieces of fiber were fused together using a microforge, thus forming a microcantilever with a V-shaped tip.

Microscope system

Cells were viewed on a Nikon inverted microscope with monochromatic illumination at 436 nm. The image from the objective was split into two

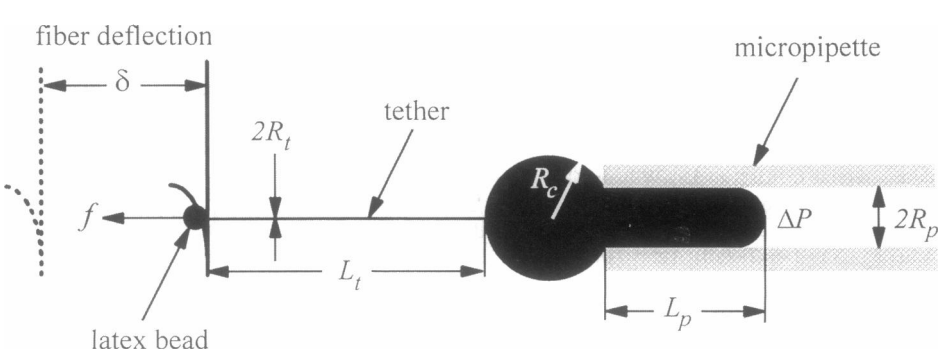

FIGURE 1 Schematic of the experiment. A tether was formed between a latex bead trapped in the crotch of a glass fiber (*left*) and a red cell aspirated into a pipette (*right*). Parameters shown in this figure include pipette radius R_p, aspiration pressure ΔP, projection inside the pipette L_p, cell radius R_c, tether radius R_t, tether length L_t, tethering force f, and the deflection (δ) of the fiber from its initial position.

images using a beam splitter. One image was further magnified to provide a clear image of the cell projection inside the pipette. The region of the magnified image could be translated across the optical field to follow the red blood cell as it traversed the field of view of the microscope. The other lower magnification image was used to observe the tether length and the deflection of the microcantilever. These two images were combined electronically along with digital readings for time and aspiration pressure to produce a single image (Fig. 2). The composite image was recorded on videotape (super VHS) for further analysis.

Microcantilever calibration

Microcantilevers were calibrated by using a large pipette (4-μm inside diameter). During the calibration, a red cell-bead pair was identified and slid into the V-shaped tip of the microcantilever. The red cell was then aspirated into the calibration pipette. The size of the pipette was large enough that the entire red cell could be aspirated into the pipette like a piston inside a cylinder. The force on the microcantilever was taken as the product of the aspiration pressure in the pipette ΔP times the cross-sectional area of the pipette:

$$f = \Delta P \cdot \pi R_p^2 \tag{1}$$

where R_p is the pipette radius. The beam constant of the microcantilever was obtained by plotting the forces for a series of aspiration pressures against the corresponding deflections of the microcantilever. To avoid adhesion between the red cell and pipette wall, autologous plasma (5% v/v) was added to the solution.

Analysis and interpretation of data

Calculation of tether radius

Tethers are too small to be resolved under an optical microscope. Therefore the tether radius was calculated from other measurable quantities. Based on conservation of area and volume, and assuming that the tether radius is constant and the portion of the cell outside the pipette is spherical, it can be shown that the tether radius is (Hochmuth and Evans, 1982)

$$R_t \cong R_p\left(-\frac{dL_p}{dL_t}\right)\left(1 - \frac{R_p}{R_c}\right) \tag{2}$$

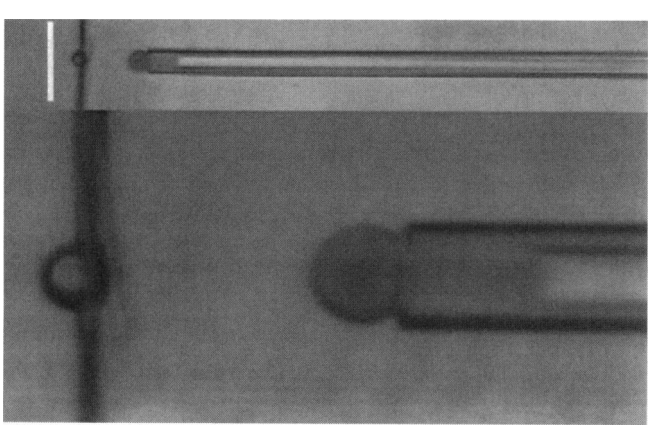

FIGURE 2 Still image obtained from an experiment. A cell aspirated into a micropipette is visible at low magnification (*upper left*) and centered in the high-magnification inset. Also visible is the latex bead caught in the tip of a glass microcantilever (*left*). A tether (invisible in this picture because of its small size) is formed between the red cell and the latex bead. The fiber is deflected from its initial position, which is indicated by the vertical white bar.

where R_t is the tether radius, R_p is the pipette radius, R_c is the cell radius, and dL_p/dL_t is the change in projection length with increasing tether length during tether formation. During force relaxation, the tether radius increases at constant tether length. This is reflected in a measurable decrease in the projection length L_p with time. Based on conservation of area and volume, and assuming the portion of the red cell outside of the pipette is spherical, the change in tether radius at constant tether length can be estimated by

$$\Delta R_t \cong \frac{R_p}{L_t}\left(1 - \frac{R_p}{R_c}\right)(-\Delta L_p) \tag{3}$$

Simulation of red blood cell contour

Under certain conditions (low aspiration pressure and large external force), the red cell contour may deviate from a sphere. To estimate how this might affect the accuracy of calculations based on Eqs. 2 and 3, numerical calculations of the membrane contour were performed. The calculations were based on membrane equations of equilibrium and on approximate constitutive models of the membrane elastic behavior (see Appendix for details). For a given tether length and tether radius, the cell projection length L_p was obtained, which satisfied the equations of equilibrium and constraints of fixed cell area and cell volume.

THEORETICAL FRAMEWORK

We assume that the free energy of the system is the sum of the contributions from external forces (the pressure and the tether force) plus elastic energy stored by the tethered cell. This elastic energy is assumed to be the sum of local and nonlocal contributions to the bending energy of the membrane bilayer plus an energy per unit area of association between the membrane bilayer and the underlying membrane skeleton (W_{sk}). This energy W_{sk} is assumed to be independent of the tether length and the tether radius. In this case, the energy of the system can be written in differential form as (Božič et al., 1992)

$$dF = \pi k_c d\left(\frac{L_t}{R_t}\right) + \gamma(L_t - L_t^*)dL_t - \pi R_p^2 \Delta P dL_p - f dL_t + W_{sk} d(2\pi R_t L_t) \tag{4}$$

where the terms on the right-hand side of Eq. 4 from left to right represent the local bending energy, the nonlocal bending energy, the work done by the aspiration pressure, the work done by the microcantilever, and the additional work required to separate the lipid bilayer from the membrane skeleton, respectively. An energy minimization approach, subject to constraints of conservation of area and volume, was used to obtain two equations to be used for calculating k_c and W_{sk}:

$$k_c = \frac{fR_t}{2\pi} - \frac{\gamma(L_t - L_t^*)R_t}{2\pi} - \frac{R_p \Delta P R_t^3}{2(R_c - R_p)} \tag{5}$$

$$W_{sk} = \frac{f}{4\pi R_t} - \frac{\gamma(L_t - L_t^*)}{4\pi R_t} + \frac{R_p \Delta P(3R_t - 2R_c)}{4(R_c - R_p)} \tag{6}$$

Equations 5 and 6 can be further simplified. In Eq. 5, because the tether radius is small, the third term on the right-hand side of the equation can be neglected. The second

term on the right-hand side of Eq. 5 arises from the nonlocal bending stiffness of the membrane and is expected to increase in proportion to the tether length. The constant of proportionality gives the value of γ. In the case that $\gamma L_t \ll f$, the second terms in Eqs. 5 and 6 can also be neglected. In this case, Eqs. 5 and 6 can be written as

$$k_c \cong \frac{fR_t}{2\pi} \tag{7}$$

$$W_{sk} \cong \frac{f}{4\pi R_t} - \frac{R_p R_c \Delta P}{2(R_c - R_p)} \tag{8}$$

The bending stiffness of the membrane k_c and separation work per unit area W_{sk} were calculated from Eqs. 5 and 6 or (when $\gamma L_t \ll f$) Eqs. 7 and 8, using measured values of the tethering force f, the pipette radius R_p, the cell radius R_c, the aspiration pressure ΔP, and the value of the tether radius R_t obtained via Eqs. 2 and 3.

RESULTS

Cell contour and the accuracy of the tether radius calculations

Numerical calculations of the cell contour were carried out as described in the Appendix. Simulations of each experiment were performed in which the initial cell dimensions and the experimental force and tether length were used as input. A value for the tether radius based on the data and Eq. 2 was chosen, and the program calculated the length of the cell projection and the shape of the cell contour outside the pipette for each force, tether length data pair. The shape of the membrane contour (Fig. 3) and the calculated projection lengths did not differ significantly from experimental observations, indicating that Eq. 2 provides a reliable estimate of tether radius for these experiments. Values of the tether radius that provided the closest agreement between calculated and measured projection lengths typically agreed within 3% with the radius calculated from the data using Eq. 2. Thus, although in principle changes in cell contour would affect the calculation of R_t, the conditions of the present experiments were such that Eq. 2 provides a reliable estimate of R_t.

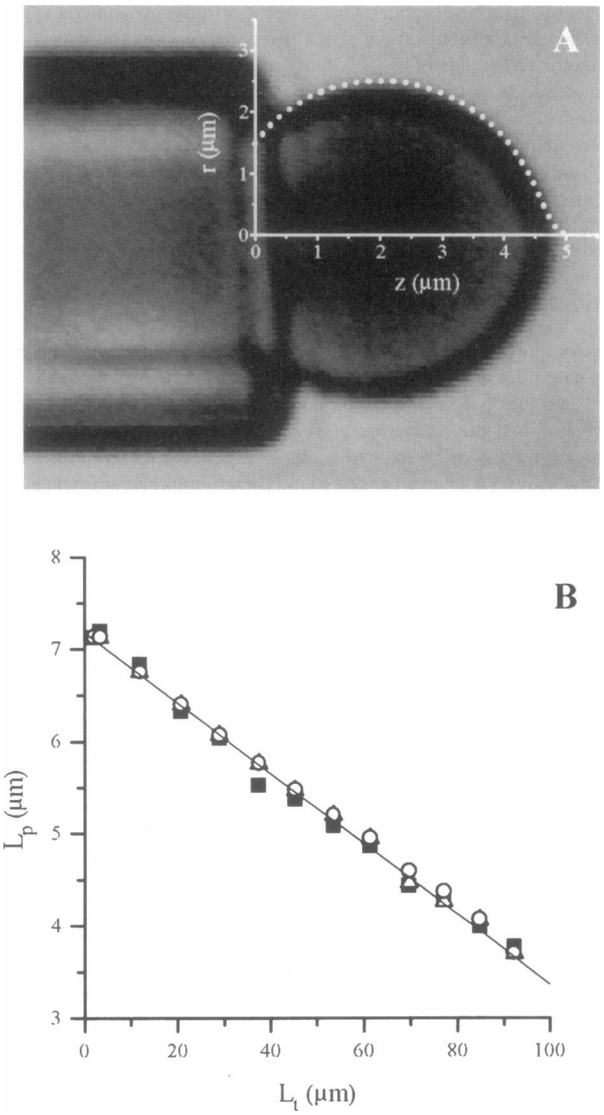

FIGURE 3 Results from red cell contour simulation. (*a*) Comparison between contour obtained from simulation and contour obtained from experiment. (*b*) L_p-L_t plot of experimental data versus simulation data. Solid squares represent experimental data. Open circle represents simulation data assuming tether radius is 23 nm. Open triangles represent simulation data assuming tether radius is 24 nm. The tether radius calculated from the data via Eq. 2 was 23.8 nm.

Results from dynamic studies

In dynamic studies of tether formation, tethers were formed at different growth rates. Tethering forces were monitored as a function of time. The tethering force increased on an apparently exponential time course as the tether grew and appeared to approach a steady-state value (Fig. 4). In general, this steady-state value increased with tether growth rate (Fig. 5). By extrapolating the steady-state force to zero tether growth rate, the steady-state force at zero tether growth rate was estimated to be 53 ± 6 pN. The tether radius was found to decrease with increasing tether growth rate. By extrapolating to zero growth rate, the value of the tether radius corresponding to the force at zero growth rate was estimated to be 26 ± 1 nm. Using these values in Eqs. 7 and 8, the separation work per unit area between the lipid bilayer and the membrane skeleton W_{sk} was evaluated to be 0.06 mJ/m^2, and the bending stiffness of the membrane k_c was found to be 2.2 ± 0.3 × 10^{-19} Nm. (Note that these calculated values do not account for possible contributions from nonlocal bending stiffness.)

Results from equilibrium studies

In equilibrium studies, tethers were first formed and then kept at constant length. The tethering force was monitored

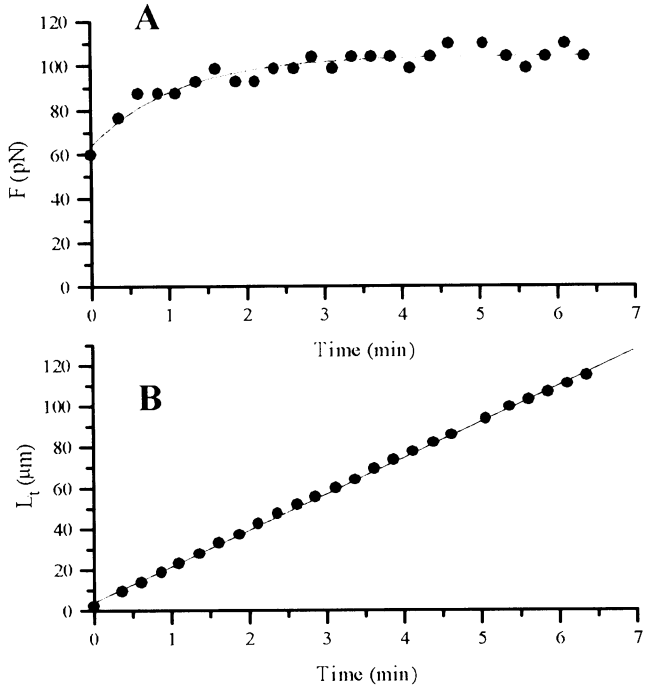

FIGURE 4 The tethering force appears to approach a steady value as the tether grows. (*Top curve*) Tethering force as a function of time. (*Bottom curve*) Tether length as a function of time. The velocity of tether growth was 0.3 μm/s, and the steady-state tethering force was estimated to be 104 pN.

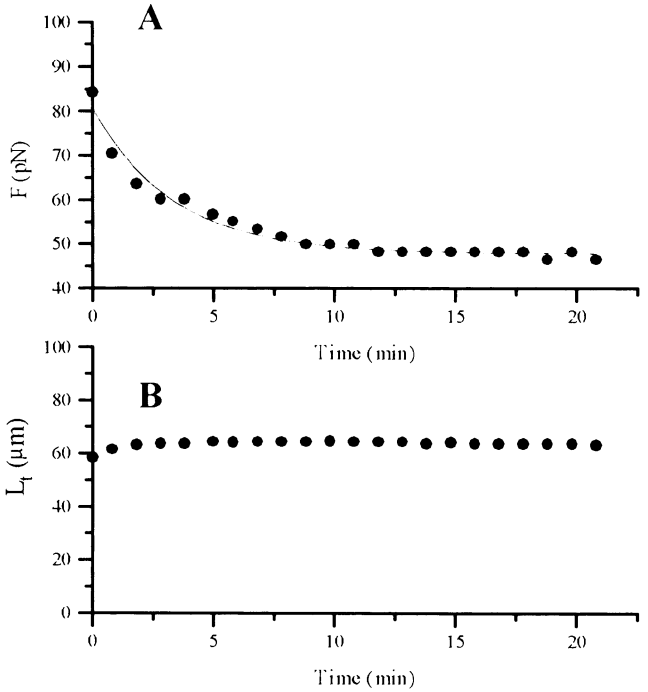

FIGURE 6 The tethering force decreases exponentially to an apparent equilibrium value during force relaxation. The relaxed force is independent of tether growth rate. (*Top curve*) Tethering force as a function of time. (*Bottom curve*) Tether length as a function of time.

as a function of time. The tethering force decreased exponentially to a steady "equilibrium" value (Fig. 6). This apparent equilibrium value ranged between 40 and 60 pN and was independent of the rate at which the tether was formed. Consistent with expectations based on Eqs. 3 and 7, as the force decreased there was a decrease in L_p indicative of an increase in tether radius. The apparent increase in R_t was calculated via Eq. 3. The equilibrium force showed a very slight dependence on the tether length at which the force relaxation was measured (Fig. 7). According to Eq. 5, this dependence of the relaxed force on tether length can be used to determine the nonlocal bending parameter γ, which reflects a contribution from the nonlocal bending stiffness of the membrane. From the data shown in Fig. 7 *a*, the value of γ was determined to be 0.11 ± 0.07 pN/μm. Using this value in Eq. 5, we obtained a mean value for k_c of 2.0 ± 0.6 × 10^{-19} J for 16 measurements of tether relaxation length ranging from 38 to 110 μm. The value of γ also affects the calculation of W_{sk} (Eq. 6). Using Eq. 6 and taking γ = 0.11 pN/μm, the mean value of W_{sk} for 16 measurements was 0.05 ± 0.04 mJ/m^2, in excellent agreement with the result obtained from dynamic studies.

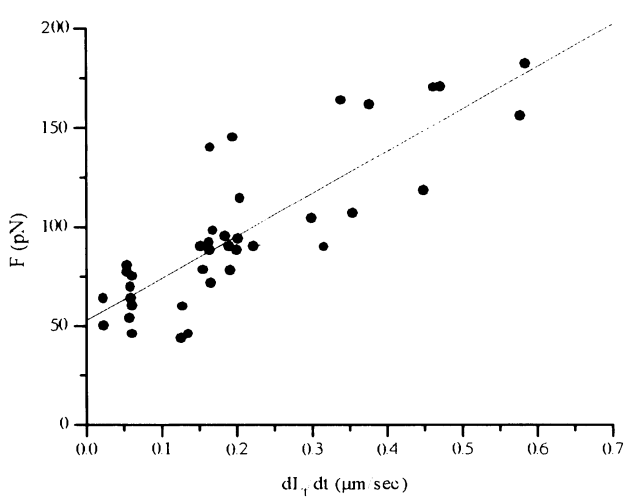

FIGURE 5 Steady-state tethering forces at various tether growth rates. Steady-state tethering forces increase with the tether growth rate. The rate of increase of equilibrium tethering force is found to be 214 ± 22 pN/(μm/s).

The dependence of the equilibrium tethering force on tether length is small, and there is considerable scatter in the data. Nevertheless, the 95% confidence interval for γ indicates that it is not zero (Fig. 7 *a*). This could result in a slight overestimation of k_c when calculated via Eq. 7, as was the case for the dynamic measurements. The contribution from the neglected term for an average tether length (~50 μm) is ~5.5 pN, or 10% of the equilibrium tethering force. Thus, neglecting the γ term in Eq. 5 might have resulted in an overestimation of k_c of approximately 10%. Taking γ into account, we estimate for the dynamic experiments that $k_c \cong 2.0 \times 10^{-19}$ J. This value is in good agreement with the value determined from relaxation measurements, in which the value of γ was included.

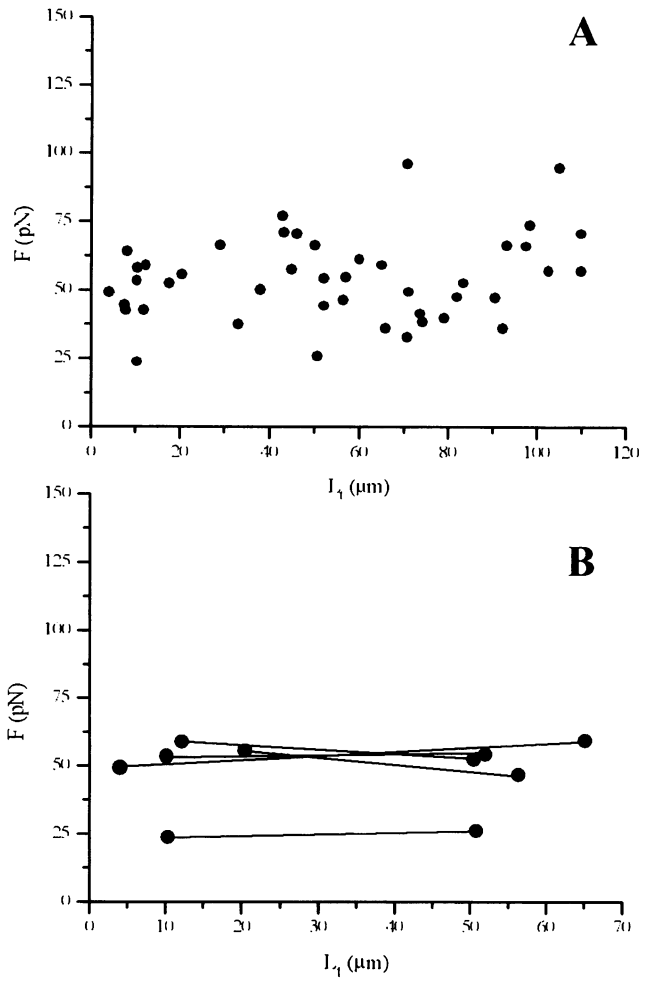

FIGURE 7 Steady-state tethering force as a function of tether length. (*a*) The slope, $df/dL_t \cong \gamma$, is 0.11 ± 0.07 pN/μm. The extrapolated value of the force at zero tether length is 48 pN. Thus for a tether 100 μm in length, the contribution to the force due to the nonlocal bending resistance is approximately 12 pN. (*b*) Force relaxations performed on the same tether and microcantilever for individual pairs. Force relaxations performed on the same tether were line-connected. The average value of the slope, $df/dL_t \cong \gamma$, is −0.04 ± 0.15 pN/μm.

We recognize the possibility that the nonzero value of the apparent nonlocal stiffness of the membrane could be the result of measurement error. We note that the longest tethers tended to be formed by using fibers with a large stiffness. The reason for this is technical: the field of view is limited, and the smaller deflection of the stiffest fibers allowed longer tethers to be formed without losing sight of the cell. Thus measurements at the shortest and longest tether lengths were generally performed on different cells using different microcantilevers. In five cases we succeeded in performing relaxation measurements on the same tether by using the same cantilever at both short and long tether lengths. For these five cases, the mean value of the γ (df/dL_t) was found to be −0.04 ± 0.15 pN/μm. While these data remain somewhat inconclusive, we cannot rule out the possibility that the effective value of γ (after periods of relaxation on the order of 10 min) may be very close to zero. Although this has major implications for understanding the role of nonlocal stiffness in determining the response of the cell membrane to prolonged deformation, the impact on our estimations of k_c and W_{sk} is relatively slight. If we take $\gamma = 0$, the calculated values are $k_c = 2.5 \pm 0.8 \times 10^{-19}$ J and $W_{sk} = 0.06 \pm 0.03$ mJ/m^2, only 25% larger than the values obtained using the value of γ obtained directly from the data in Fig. 7.

DISCUSSION

These data provide the first definitive measurements of the contribution of the red cell membrane skeleton to the stabilization of the red cell membrane against loss of surface through the preferential loss of membrane bilayer. A previous study of tether formation from red cells in this laboratory focused on ultrastructural aspects of tether formation and provided evidence that the formation of tethers involves separation of bilayer from the underlying membrane skeleton and lateral segregation of some integral membrane components (Waugh and Bauserman, 1995). The segregation of bilayer from skeleton appears to be absolute. Band 3, which has been shown to follow the distribution of the underlying membrane skeleton (Discher et al., 1994), was not detectable in tethers labeled with eosin maleimide, a fluorophore that labels band 3 preferentially (Waugh and Bauserman, 1995). Furthermore, treatment of tethered cells with the detergent Triton X-100 and subsequent examination by electron microscopy revealed the complete destruction of the tether structure, whereas the membrane skeleton associated with the main body of the cell was clearly evident (Waugh and Bauserman, 1995). Other evidence indicates that at least some integral protein finds its way into the tether (Berk and Hochmouth, 1992), but which proteins and at what surface concentration remains a subject of investigation. Nevertheless, all available evidence indicates that there are no membrane skeletal components in the tether.

In our previous work, preliminary estimates of the work of tether formation were made, but these measurements could not be interpreted unambigously because the dependence of the tethering force on tether length was not known. Measurements of the length dependence of the equilibrium tethering force presented here make it possible to distinguish clearly between contributions to the work of tether formation due to the bending rigidity of the membrane bilayer and contributions due to the presence of the membrane skeleton and integral membrane proteins. The reader should also note that the separation work defined in our former publication is somewhat different from W_{sk} as defined in Eq. 4 of the present work. Specifically, the former definition included all contributions to the work of tether formation, including both elastic and dissipative contributions and the work required to deform (bend) the membrane bilayer. In the present work, W_{sk} represents only the elastic component of the work required to separate bilayer and

skeleton, and does not include the work required to bend the membrane bilayer. Thus the values of W reported in the two papers are not directly comparable, but for the equilibrium case they are related by

$$W_{sk} = W_s - \frac{k_c}{2R_t^2}$$

where W_s represents the "elastic" contribution to the work reported previously. Taking $k_c = 2.3 \times 10^{-19}$ J and $R_t = 28$ nm, and using the value reported previously for W_s (0.22 mJ/m^2), we obtain a value for W_{sk} of 0.07 mJ/m^2, in good agreement with the values obtained in the present, more extensive study.

These measurements also provide the first measurements of the so-called nonlocal bending stiffness of red cell membrane, a quantity that heretofore has only been estimated theoretically (Waugh and Hochmuth, 1987). According to theory, assuming no exchange of molecules between the two leaflets, the nonlocal bending stiffness of the membrane k_r is related to the area expansivity modulus of the membrane by (Waugh et al., 1992b)

$$k_r = \frac{Kh^2}{4} \tag{9}$$

where K is the area expansivity modulus of the membrane and h is the separation distance between the neutral surfaces of the two leaflets. The area expansivity modulus for red cells, $K \cong 500$ mN/m, and the separation distance, $h \cong 2.5$ nm, indicate that the nonlocal bending stiffness k_r would be $\cong 7.8 \times 10^{-19}$ J. The nonlocal bending modulus of the membrane k_r is related to the nonlocal bending parameter γ by

$$k_r = \frac{\gamma A}{4\pi^2} \tag{10}$$

where A is the total area of the membrane (Waugh et al., 1992b). Based on a total area of the red cell membrane of $\cong$ 135 μm^2 (Fung et al., 1981), and using the experimentally determined value of γ, we obtain $k_r = 3.8 \times 10^{-19}$ J. The fact that the measured nonlocal bending stiffness was smaller than predicted from theory suggests that the leaflet strains resulting from the area difference between the two leaflets of bilayer induced by tether formation may have been relaxed during tether formation, possibly by a net transport of molecules between the membrane leaflets. There is evidence that cholesterol can move rapidly from one leaflet to the other (Lange et al., 1981), and this could account in part for the relaxation. Another possibility is that passive exchange of lipid molecules between leaflets may be accelerated because of the presence of facilitating integral membrane proteins (Devaux, 1992) or because of the stress difference between the leaflets that arises as a result of tether formation. Evidence for such accelerated transbilayer movements of lipid molecules in phospholipid membranes subjected to mechanical stress has recently been reported (Raphael and Waugh, 1996).

The forces required to form tethers from red cells are significantly greater than forces of tether formation that have been measured in pure phospholipid vesicles (Raphael and Waugh, 1996) or forces required to form tethers from neuronal growth cone membranes (Dai and Sheetz, 1995). The difference between tethering forces for bilayer vesicles and for red cells provides direct evidence of the important role of the red cell membrane proteins in preventing loss of membrane bilayer by fragmentation or vesiculation. Tethering forces for red cells (~50–60 pN) are approximately an order of magnitude larger than tethering forces for neuronal growth cone membrane (~5 pN), indicating that differences in the properties of the membrane-associated cytoskeleton and the nature of the association between the bilayer and underlying structural components in these cell types have enormous effects on membrane stability. Interestingly, the forces we report here for red cells are nearly identical to those recently reported by Shao and Hochmuth for neutrophils (Shao and Hochmuth, 1996). This similarity may be coincidental or it may report a common "design" of these membranes to resist surface loss as a result of hydrodynamic forces or adhesive interactions in the circulation.

Although the precise mechanisms responsible for determing the strength of the bilayer-skeletal association remain obscure, quantitative measurements of the work of separation provide important insights into the possible mechanisms responsible for this association. The measured work of dissociation (0.06 mJ/m^2) is 3–7 times larger than the adhesive energy density between phospholipid membranes mediated by van der Waals interaction alone (Evans and Metcalfe, 1984), and yet is significantly smaller than adhesion mediated by receptor-ligand interactions at moderate density (Evans et al., 1991; Leckband et al., 1995). One possible origin of this additional contribution is a chemical potential difference generated by the segregation of membrane proteins (for example, band 3) between the tether and the cell body during tether formation. It was estimated that complete segregation of band 3 proteins would correspond to an energy of tether formation of 0.16 mJ/m^2 (Waugh and Bauserman, 1995). Given the large number and diversity of integral proteins present in the red cell membrane, and evidence that many of these undergo lateral redistribution in deformed membranes (Discher et al., 1994), this remains as a possible mechanism for the additional energy costs we have observed. Other mechanisms, such as the elastic deformation of the membrane skeleton near the cell-tether junction, may also play a role.

The present work provides quantitative measurement of the bilayer-skeletal dissociation energy for normal red cell membranes. Previous measurements indicate that this association can be markedly reduced in abnormal red cells (Waugh and Agre, 1988). Although the mechanisms responsible for the association between the lipid bilayer and the membrane skeleton remain obscure, quantitative measurements of this association energy such as those performed in

this study are expected to provide definitive insights into the mechanisms of membrane stabilization in future studies on chemically modified or abnormal membrane.

APPENDIX: NUMERICAL CALCULATION OF RED CELL CONTOUR

The shape of the red cell contour was calculated based on the equations of membrane equilibrium. In the cell body region, the cell radius is much larger than the thickness of the membrane. As a result, the bending contribution to the force balance is negligible in this region, and shear elasticity alone is sufficient to reproduce the red cell contour satisfactorily, although very near the tether region accurate representation of the cell contour may require taking the bending contribution into account. In the present case, in which we are concerned only with the area and volume of the contour, bending stiffness is neglected.

The axial and tangential equations of mechanical equilibrium for an axisymmetrical membrane are, respectively (Hochmuth and Evans, 1982),

$$2\pi r T_m \sin\theta = (P_c - P_o)\pi r^2 + f \tag{A1}$$

and

$$r\frac{\partial T_m}{\partial s} + (T_m - T_\phi)\frac{\partial r}{\partial s} = 0 \tag{A2}$$

where T_m is the membrane tension in the meridional direction, T_ϕ is the membrane tension in the circumferential direction, P_c the pressure inside the red cell, P_o is the pressure outside of the red cell, f is the tethering force, r is the radial coordinate, and θ is the angle between the surface normal of the membrane and the axis of symmetry (Fig. 8).

The quantity $(T_m - T_\phi)$ is two times the membrane surface shear resultant, which is constitutively related to the surface deformation. Although recent evidence shows clearly that deformation of the membrane skeleton involves both shear and dilational components (Discher et al., 1994), for purposes of calculation in the present analysis, the simpler, incompressible approximation of membrane elasticity is used. Although it is not a perfect description of the deformation of the membrane skeleton, this model does provide a reasonable approximate description of the membrane behavior, and it vastly simplifies calculation of the membrane strain. In this case, the shear resultant T_s is related to the membrane deformation by

$$T_s \equiv \frac{T_m - T_\phi}{2} \equiv \frac{\mu}{2}(\lambda_m^2 - \lambda_\phi^2) \tag{A3}$$

Substituting this expression into Eq. A2, and recognizing that $dr/ds = \cos\theta$, we obtain the tangential force balance in the form

$$\frac{dT_m}{ds} = -\frac{\mu}{r}(\lambda_m^2 - \lambda_\phi^2)\cos\theta \tag{A4}$$

where μ is the membrane shear elasticity modulus, and λ_m, λ_ϕ are the surface extension ratios in the meridional and circumferential directions, respectively.

Combining Eqs. A1 and A4 to eliminate T_m, it can be shown that

$$\frac{d\theta}{ds} = \frac{\left(2P_w\sin\theta - \frac{(f + P_w\pi r^2)\sin\theta}{\pi r^2}\right) - \left(\frac{2\mu\sin^2\theta(\lambda_m^2 - \lambda_\phi^2)}{r}\right)}{(P_w r + f/\pi r)} \tag{A5}$$

where $P_w \equiv P_c - P_o$. From geometry, we have

$$\frac{dz}{ds} = \sin\theta \tag{A6}$$

$$\frac{dr}{ds} = \cos\theta \tag{A7}$$

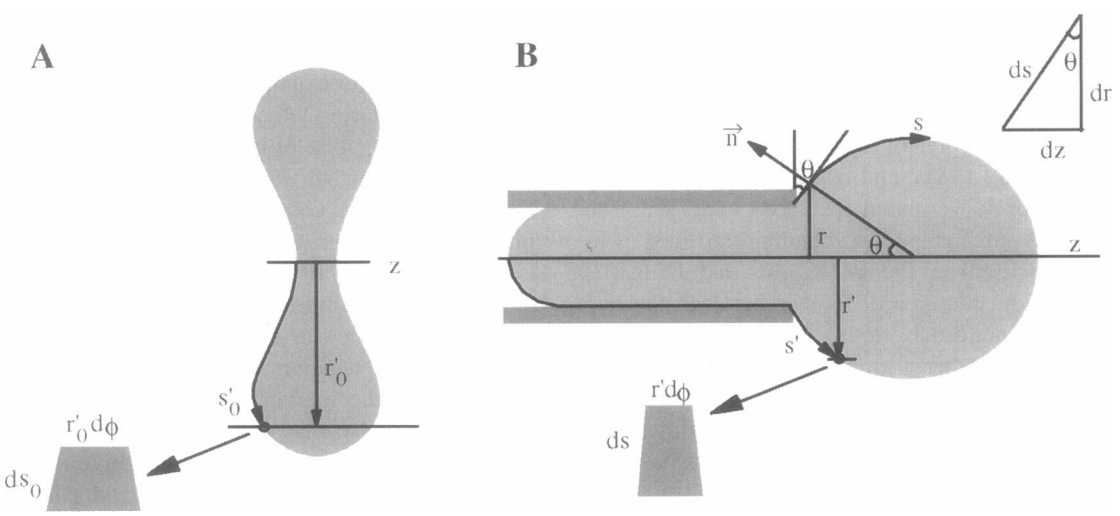

FIGURE 8 Coordinates in red cell contour simulation. (*a*) Coordinate in the undeformed (reference) state. The distance along the surface is s_0, and the radial coordinate is r_0. The system is assumed to be symmetrical about the z axis. (*b*) Coordinate in the deformed state. The surface normal, $\vec{n}$, makes an angle θ with the z axis. The distance along the surface is s, and the radial coordinate is r. The system is assumed to be symmetrical about the z axis. Also shown is the mapping of a material element from its location in the undeformed state (r'_0, s'_0) to its location in the deformed state (r', s'). The material deformation is defined in terms of the extension ratios: $\lambda_m = ds/ds_0$ and $\lambda_\phi = r/r_0$. For an incompressible surface, the mapping is achieved by equating the areas of the deformed and undeformed membranes.

For an incompressible axisymmetrical membrane, the extension ratios are related to the radial coordinates in the deformed (r) and undeformed (r_0) geometries (Fig. 8):

$$\lambda_m = \frac{r_0}{r} \tag{A8}$$

$$\lambda_\phi = \frac{r}{r_0} \tag{A9}$$

The reference state of the red blood cell contour is taken to be a biconcave disk, which can be described by the following (Fung et al., 1981):

$$T(x) = (1 - x^2)^{1/2}(c_0 + c_1x^2 + c_2x^4) \tag{A10}$$

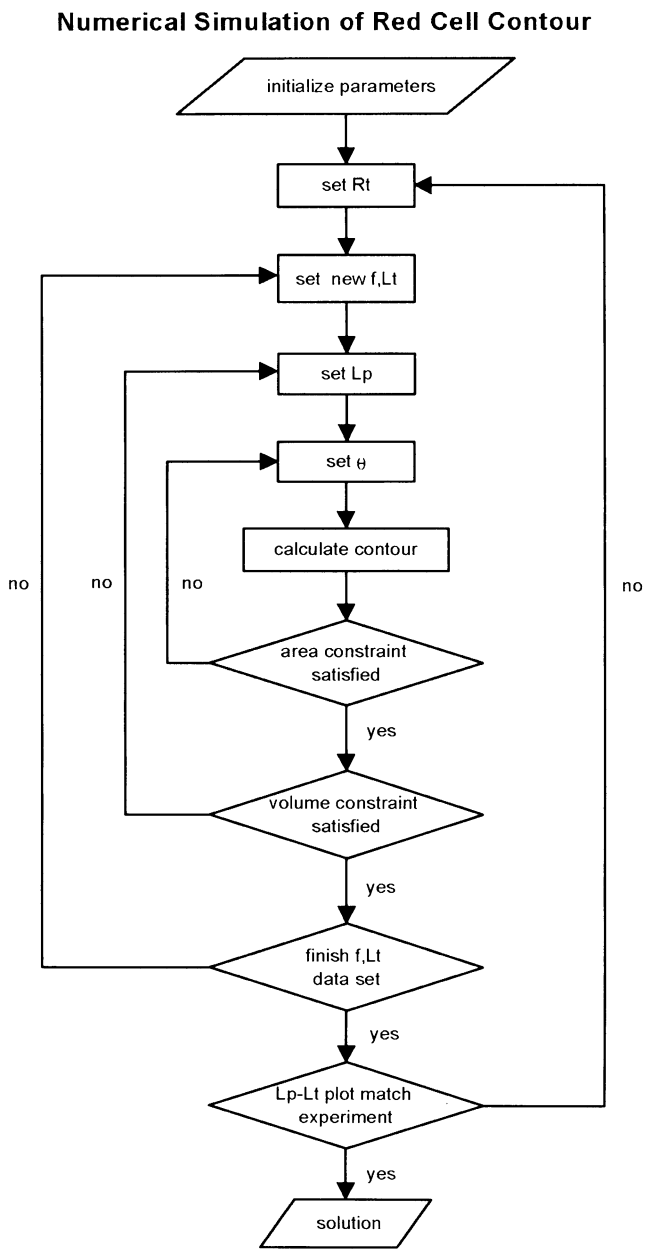

FIGURE 9 Flow diagram of algorithm for numerical simulation of red blood cell contour.

where $T(x)$ is the half-thickness of the red cell; $x \equiv r_0/R_0$; r_0 is the radial coordinate; R_0 is the radius of the cell; and c_0, c_1, c_2 are constants. Published values of these coefficients based on optical interference measurements of the thickness are $c_0 = 0.405$ μm, $c_1 = 3.915$ μm, and $c_2 = -2.195$ μm, respectively (Evans and Fung, 1972). The surface area of the reference state red blood cell contour is simply

$$A = 4\pi R_0^2 \int_0^1 x\left(1 + \left(\frac{1}{R_0}\frac{dT}{dx}\right)^2\right)^{1/2} dx \tag{A11}$$

Numerical integration of Eqs. A5, A6, and A7 was performed using a fourth-order Runge-Kutta algorithm. The logical flow of the calculations is diagrammed in Fig. 9. The starting point for the integration was the intersection of the cell contour with the opening of the pipette. The cell area and volume were specified, and the radius of the resting cell shape was chosen such that the area given by Eq. A11 matched the specified area. The pipette radius was specified, and a trial value of the projection length L_p was chosen. The extension ratios were calculated at each step via Eqs. A8 and A9, where the undeformed radius r_0 was obtained by equating the area of the undeformed geometry corresponding to r_0 with the area of the deformed geometry, including the projection length plus the integrated area of the contour up to the surface location of interest. Integration stopped when $r = R_t$ or when the area of the trial contour exceeded the specified cell area.

Trial contours were generated for different starting values of the surface angle θ. The starting angle θ was adjusted to obtain a closed contour with the correct area. Then the projection length of the cell was adjusted to obtain the correct cell volume. The procedure was repeated iteratively, adjusting the starting value for θ and the projection length L_p until a closed contour with the specified area and volume was obtained.

This procedure was repeated for each set of experimental conditions. To simulate tether growth, the initial cell area was reduced by $2\pi R_t L_t$, where R_t was the trial value of the tether radius and f and L_t were assigned successive values obtained from experiment. The computed values for L_p as a function of tether length were compared with experiment, and the value of R_t was adjusted until a match was found.

The authors thank Mrs. Donna Brooks and Mr. Richard Bauserman for technical support.

This work was supported by the U.S. Public Health Service under NIH grants HL18208 and HL31524.

REFERENCES

Bennett, V., and P. Stenbuck. 1979. The membrane attachment protein for spectrin is associated with band 3 in human erythrocyte membranes. *Nature.* 280:468–473.

Berk, D. A., and R. Hochmouth. 1992. Lateral mobility of integral proteins in red cell tethers. *Biophys. J.* 61:9–18

Božič, B., S. Svetina, B. Žekš, and R. Waugh. 1992. Role of lamellar membrane structure in tether formation from bilayer vesicles. *Biophys. J.* 61:963–973.

Dai, J., and M. Sheetz. 1995. Mechanical properties of neuronal growth cone membrane studied by tether formation with laser optical tweezers. *Biophys. J.* 68:988–996.

Devaux, P. 1992. Protein involvement in trasnmembrane lipid asymmetry. *Annu. Rev. Biophys. Biomol. Struct.* 21:417–439.

Discher, D. E., N. Mohandas, and E. Evans. 1994. Molecular maps of red cell deformation: hidden elasticity and in situ connectivity. *Science.* 266:1032–1035.

Evans, E., D. Berk, and A. Leung. 1991. Detachment of agglutinin-bonded red blood cells. I. Forces to rupture molecular-pointed attachments. *Biophys. J.* 59:838–848.

Evans, E., and Y. C. Fung. 1972. Improved measurements of the erythrocyte geometry. *Microvasc. Res.* 4:335–347.

Evans, E., and M. Metcalfe. 1984. Free energy potential for aggregation of mixed phosphatidylcholine/phosphatidylserine lipid vesicles in glucose polymer (dextran) solutions. *Biophys. J.* 45:715–720.

Fung, Y. C., W. O. Tsang, and P. Patitucci. 1981. High resolution data on the geometry of red blood cells. *Biorheology.* 18:369–385.

Hochmuth, R. M., and E. Evans. 1982. Extensional flow of erythrocyte membrane from cell body to elastic tether. I. Analysis. *Biophys. J.* 39:71–81.

Lange, Y., J. Dolde, and T. Steck. 1981. The rate of transmembrane movement of cholesterol in the human erythrocyte. *J. Biol. Chem.* 256:5321–5323.

Leckband, D., W. Muller, F.-J. Schmitt, and H. Ringsdorf. 1995. Molecular mechanisms determing the strength of receptor-mediated intermembrane adhesion. *Biophys. J.* 69:1162–1169.

Palek, J., and S. Lambert. 1990. Genetics of the red cell membrane skeleton. *Semin. Hematol.* 27:290–332.

Pinder, J., A. Chung, M. Reid, and W. B. Gratzer. 1993. Membrane attachment sites for the membrane cytoskeletal protein 4.1 of the red blood cell. *Blood.* 82:3482–3488.

Raphael, R., and R. Waugh. 1996. Accelerated interleaflet transport of phosphatidylcholine molecules in membranes under deformation. *Biophys. J.* 71:1374–1388.

Shao, J., and R. Hochmuth. 1996. Micropipette suction for measuring piconewton forces of adhesion and tether formation from neutrophil membranes. *Biophys. J.* 71:2892–2901.

Waugh, R., and P. Agre. 1988. Reduction of erythrocyte membrane viscoelastic coefficients reflect spectrin deficiencies in hereditary spherocytosis. *J. Clin. Invest.* 81:133–141.

Waugh, R., and R. Bauserman. 1995. Physical measurements of bilayer-skeletal separation forces. *Ann. Biomed. Eng.* 23:308–321.

Waugh, R., and R. Hochmuth. 1987. Mechanical equilibrium of thick, hollow, liquid membrane cylinders. *Biophys. J.* 52:391–400.

Waugh, R., N. Mohandas, C. Jackson, T. Mueller, T. Suzuki, and G. Dale. 1992a. Rheologic properties of senescent erythrocytes: loss of surface area and volume with red blood cell age. *Blood.* 79:1351–1358.

Waugh, R., J. Song, S. Svetina, and B. Žekš. 1992b. Local and nonlocal curvature elasticity in bilayer membranes by tether formation from lecithin vesicles. *Biophys. J.* 61:974–982.